Neurocomputing 197 (2016) 212–220

Contents lists available at ScienceDirect

Neurocomputing

journal homepage: www.elsevier.com/locate/neucom

Feature extraction using dual-tree complex wavelet transform and gray level co-occurrence matrix

Peng Yang*, Guowei Yang

School of Information Engineering, Nanchang Hangkong University, Jiangxi, China

ARTICLE INFO

Article history:
Received 23 November 2015
Received in revised form
24 January 2016
Accepted 8 February 2016
Available online 15 March 2016

Keywords:
Feature extraction
Texture classification
Dual-tree complex wavelet transform
Gray level co-occurrence matrix

ABSTRACT

This paper introduces a new feature extraction method for texture classification application. In the proposed method, dual-tree complex wavelet transform is first performed on the original image to obtain sub-images at six directions. After that gray level co-occurrence matrix of each sub-image is calculated and the corresponding statistical values are used to construct the final feature vector. The experimental results demonstrate that our proposed method has the property of robustness, and can achieve higher texture classification accuracy rate than the conventional methods.

1. Introduction

Texture classification aims to assign an unknown sample image to one of a set of known texture classes, which is fundamental to many applications such as automatic industrial inspection, biomedical image processing, aerial imagery segmentation and content based image retrieval. To obtain better classification performance, it is essential to extract texture features with good discrimination power. A number of feature extraction methods have been proposed over the years, which can be classified into three main categories: i.e., model based methods, statistical methods and signal processing methods [1].

Haralick et al. introduced the concept of gray level co-occurrence matrix (GLCM), and extracted statistical features for texture image classification [2]. As a traditional statistical feature extraction method, GLCM has been commonly used in many applications. Partio et al. applied GLCM for rock texture image retrieval, and the results showed that the GLCM features outperform Gabor wavelet features [3]. Wu et al. employed GLCM to extract the texture features of aerial insulator images for segmentation [4], and Wang et al. employed GLCM for 18 different fruit category identification [5]. Siqueira et al. extended the GLCM to multiple scales through Gaussian scale-space representation and image pyramid, which outperforms the original GLCM for texture description [6]. Furthermore, Subrahmanyam et al. presented the modified GLCM for color image retrieval [7]. Note that GLCM features can also be extracted from transformed image instead of original image. Jhanwar et al. presented a content based image retrieval system by using motif co-occurrence matrix (MCM) derived from the motif transformed image [8]. Since MCM captures the third order image statistics in the local neighborhood, it is better than the conventional methods for feature extraction. Zhang et al. first obtained GLCM from Prewitt edge images, and then calculated statistical parameters of GLCM to generate feature vector [9]. Moreover, several researchers tried to enhance the GLCM based method by fusing other extracted features [10,11].

The favorite signal processing method for feature extraction includes Gabor, wavelet transform, Contourlet, etc. Gabor filters have been used for texture segmentation, and perfect reconstruction of the input image can be achieved [12]. The energies calculated in a window around each pixel can be taken as texture features. Moreover, Gabor wavelets have been applied for rotation invariant texture classification [13,14]. The input image can be first decomposed into multiple scales and orientations. After that, texture features could be extracted by calculating the mean and variance of the Gabor filtered image. Besides using Gabor feature, Irtaza et al. introduced hybrid texture features to maximize the performance of image retrieval [15]. Ganesan et al. proposed wavelet based method by using an integration of the crude wavelets with rotational invariance [16,17]. In such method, the first- and second-order statistical parameter and entropy were calculated as texture features. Note that the consistent estimator of texture model parameters could also been applied for feature extraction, which may provide greater accuracy and flexibility in capturing texture information [18,19]. Moreover, several researchers applied discrete wavelet transform (DWT) and other

* Corresponding author.
E-mail address: pengyang@nchu.edu.cn (P. Yang).

http://dx.doi.org/10.1016/j.neucom.2016.02.061
0925-2312/

approaches jointly to extract more meaningful texture features [20–22]. Since the Contourlet transform overcomes the limitation of DWT in capturing the geometry of image edges, it could be applied to capture some smooth features (such as the contours and lines in image) [23–25]. Kingsbury et al. proposed the dual-tree complex wavelet transform (DTCWT), which has the advantages of efficient computation, approximately shift invariance and good directional selectivity [26,27]. Therefore, it can effectively address the problem of conventional Gabor filters and DWT. Celik et al. applied DTCWT for texture classification [28]. In their proposed method, feature vector was constituted by variance and entropy at multiple scales and directional sub-bands of the transformed domain. Furthermore, Kennel et al. extracted representative texture features by computing textons obtained from DTCWT decomposition [29].

In this paper, we proposed a new feature extraction method for effective and efficient texture classification. DTCWT was first used to decompose the texture image into sub-images at different directions. After that, GLCMs of each sub-image were calculated, and the statistical features of GLCMs were extracted for final classification. Since the proposed method utilizes both local mutual occurrence of patterns and global directional texture information, one can obtain elaborate description of texture image. The rest of this paper is organized as follows. Section 2 gives brief review of DTCWT and GLCM. The proposed feature extraction method is described in Section 3. Section 4 analyzes the experimental results and Section 5 addresses the conclusion.

2. DTCWT and GLCM

2.1. DTCWT

DWT suffers from the drawback of shift variance, i.e., a small shift of the input signal causes significant fluctuations in energy distribution of wavelet coefficients. Kingsbury has proposed DTCWT to address the problem, which calculates the complex transform of a signal using two separate DWT decompositions (tree a and tree b) [26]. If the filters used in one tree are specifically designed different from those in the other, it is possible for the first DWT to produce the real coefficients and the second DWT to produce the imaginary coefficients. In DTCWT, an image signal $f(x, y)$ is decomposed by using a complex scaling function and six complex wavelet functions as follow

$$f(x,y)=\sum_{l\in Z^2}A_{j_0,l}\phi_{j_0,l}(x,y)+\sum_{k\in\alpha}\sum_{j=1}^{j_0}\sum_{l\in Z^2}D_{j,l}^{k}\varphi_{j,l}^{k}(x,y) \tag{1}$$

where j_0 is the number of decomposition level,$A_{j_0,l}$ and $D_{j,l}^{k}$ are scaling coefficients and wavelet coefficients respectively. $\phi_{j_0,l}(x,y)$ denotes the scaling function and $\varphi_{j,l}^{k}(x,y)$ denotes six wavelet functions which are oriented at $k\in\alpha=\{\pm\pi/12,\pm\pi/4,\pm5\pi/12\}$. Therefore, it can produce six directionally selective sub-bands for each scale. The impulse responses of the filters for the six directional sub-bands are shown in Fig. 1.

Considering the two-dimensional wavelet $\varphi(x,y)=\varphi(x)\varphi(y)$ associated with the row–column implementation of the wavelet transform, if $\varphi_g(t)$ is approximately the Hilbert transform of $\varphi_h(t)$, i.e., $\varphi_g(t)\approx H\{\varphi_h(t)\}$, one can obtain the following six wavelets:

$$\varphi_i(x,y)=\frac{1}{\sqrt{2}}(\varphi_{1,i}(x,y)-\varphi_{2,i}(x,y)) \tag{2}$$

$$\varphi_{i+3}(x,y)=\frac{1}{\sqrt{2}}(\varphi_{1,i}(x,y)+\varphi_{2,i}(x,y)) \tag{3}$$

for $i=1$, 2, and 3, where the two separable two-dimensional wavelet bases are defined as follows:

$$\varphi_{1,1}(x,y)=\phi_h(x)\varphi_h(y),\ \varphi_{2,1}(x,y)=\phi_g(x)\varphi_g(y) \tag{4}$$

$$\varphi_{1,2}(x,y)=\varphi_h(x)\phi_h(y),\ \varphi_{2,2}(x,y)=\varphi_g(x)\phi_g(y) \tag{5}$$

$$\varphi_{1,3}(x,y)=\varphi_h(x)\varphi_h(y),\ \varphi_{2,3}(x,y)=\varphi_g(x)\varphi_g(y) \tag{6}$$

In fact, the DTCWT is implemented by taking sum/difference of two separable wavelet filter banks in a quad-tree structure with 4:1 redundancy [27]. Since each of the above six wavelets are aligned along a specific direction, the DTCWT can capture more image information than the conventional wavelet transform.

2.2. GLCM

GLCM has been introduced by Haralick, which transforms an image into a matrix according to the relationship of pixels in the original image. The mutual occurrence of pixel pairs for a specific distance oriented at a particular direction need to be calculated. After that, the statistical features can be extracted for texture image classification [5]. The GLCM with distance d and orientation θ of a $N_x\times N_y$ image is defined as $G_d^{\theta}=[g_d^{\theta}(i,j)]_{q\times q}$, where q is the gray level quantization. The elements of the GLCM with four orientations can be calculated as follows

$$g_d^0(i,j)=\#\{((k,l),(m,n))|\,k-m=0,|l-n|=d,I(k,l)=i,I(m,n)=j\} \tag{7}$$

$$g_d^{\pi/4}(i,j)=\#\{((k,l),(m,n))|k-m=d,|l-n|=d\text{ or }k-m=-d,|l-n|=-d,I(k,l)=i,I(m,n)=j\} \tag{8}$$

$$g_d^{\pi/2}(i,j)=\#\{((k,l),(m,n))|\,|k-m|=d,l-n=0,I(k,l)=i,I(m,n)=j\} \tag{9}$$

$$g_d^{3\pi/4}(i,j)=\#\{((k,l),(m,n))|k-m=d,l-n=-d\text{ or }k-m=-d,l-n=d,I(k,l)=i,I(m,n)=j\} \tag{10}$$

where $(k,l),(m,n)\in N_x\times N_y$. $I(k,l)$ and $I(m,n)$ are the pixel intensity at position (k,l) and (m,n) of the input image.

Fig. 2 shows an example of GLCM calculation. In Fig. 2 (a) original 4×4 image with 4 (from 0 to 3) gray levels is shown. G_1^0, $G_1^{\pi/4}$ and $G_1^{\pi/2}$ can be calculated according to Eqs. (7)–(9) respectively, and the results are shown in Fig. 2(b)–(d).

3. The Proposed feature extraction method

As mentioned in Section 2, DTCWT has property of good directional selectivity, which can decompose the texture image from

Fig. 1. Impulse response of DTCWT filters at different directions. (a) $-5\pi/12$, (b) $-\pi/4$, (c) $-\pi/12$, (d) $\pi/12$, (e) $\pi/4$, and (f) $5\pi/12$.

a
$$\begin{bmatrix} 0 & 0 & 0 & 2 \\ 0 & 0 & 2 & 2 \\ 1 & 1 & 2 & 3 \\ 1 & 1 & 2 & 3 \end{bmatrix}$$
b
$$\begin{bmatrix} 6 & 0 & 2 & 0 \\ 0 & 4 & 2 & 0 \\ 2 & 2 & 2 & 2 \\ 0 & 0 & 2 & 0 \end{bmatrix}$$
c
$$\begin{bmatrix} 2 & 1 & 3 & 0 \\ 1 & 2 & 1 & 0 \\ 3 & 1 & 0 & 2 \\ 0 & 0 & 2 & 0 \end{bmatrix}$$
d
$$\begin{bmatrix} 4 & 2 & 1 & 0 \\ 2 & 4 & 0 & 0 \\ 1 & 0 & 6 & 1 \\ 0 & 0 & 1 & 2 \end{bmatrix}$$

Fig. 2. GLCM example (a) The grayscale matrix of the original image. (b) GLCM with $\theta=0$ and $d=1$ (c) GLCM with $\theta=\pi/4$ and $d=1$ (d) GLCM with $\theta=\pi/2$ and $d=1$.

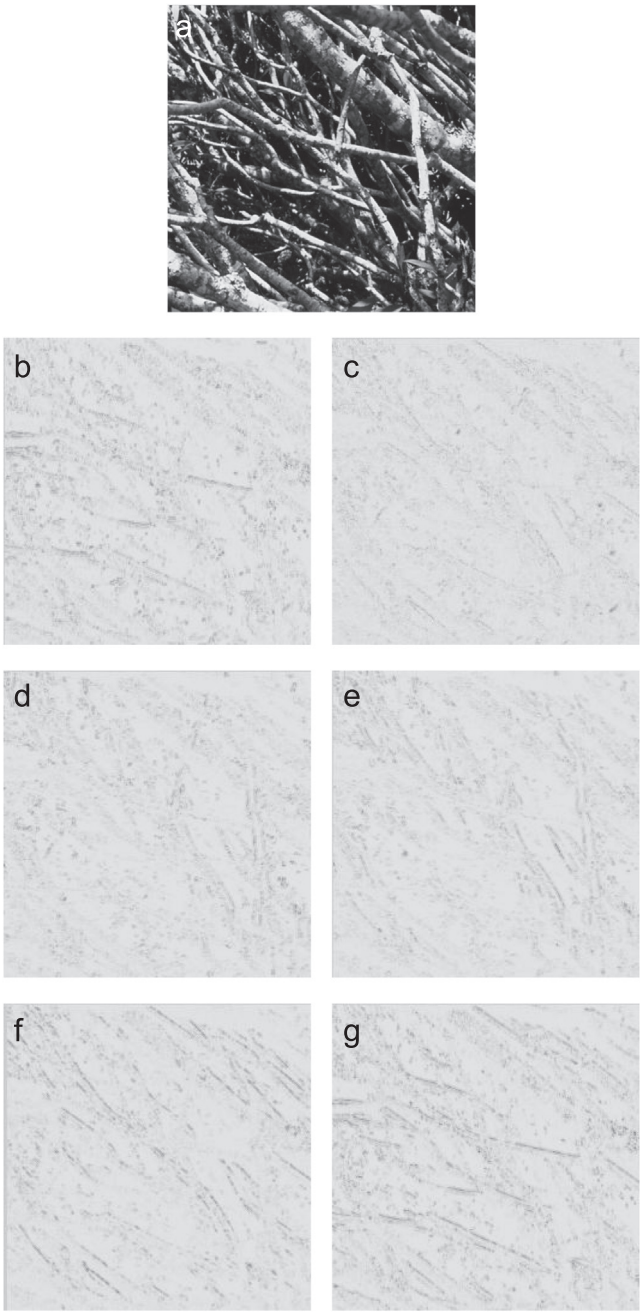

Fig. 3. DTCWT decomposition (a) original image (b) sub-image at $\pi/12$ (c) sub-image at $\pi/4$. (d) sub-image at $5\pi/12$ (e) sub-image at $-5\pi/12$ (f) sub-image at $-\pi/4$ (g) sub-image at $-\pi/12$.

multiple directions and obtain more comprehensive description of the feature information. Moreover, GLCM works directly with intensity of image, which can consider information regarding the mutual occurrence of patterns. Therefore, we try to extract features in an improved manner by keep advantages of the above two tools. In our proposed method, 1-level DTCWT is first implemented to decompose the original image. One can obtain highpass complex coefficients to construct six sub-images oriented at $\pm\pi/12$, $\pm\pi/4$ and $\pm5\pi/12$ respectively. The process is illustrated in Fig. 3.

After that, GLCMs can be calculated for the sub-images result from DTCWT decomposition. Since the selection of directions and distances in GLCM affects the discrimination power of extracted features, different combinations have been used to obtain proper GLCM (see Section 4). For a GLCM with size of $q \times q$ (q is the gray level quantization), we do not directly create a $q \times q$ feature vector. Instead, the following statistical features of GLCM, i.e., uniformity (*UNI*), contrast (*CON*), entropy (*ENT*), and inverse difference (*INV*), are calculated to describe the texture information.

$$UNI = \sum_{i=1}^{q}\sum_{j=1}^{q}\{g(i,j)\}^2 \tag{11}$$

$$CON = \sum_{n=0}^{q-1} n^2 \left\{ \sum_{i=1}^{q}\sum_{j=1}^{q} g(i,j) \right\} \text{ where } |i-j| = n \tag{12}$$

$$ENT = -\sum_{i=1}^{q}\sum_{j=1}^{q} g(i,j)\log\{g(i,j)\} \tag{13}$$

$$INV = \sum_{i=1}^{q}\sum_{j=1}^{q} g(i,j)/\{1+(i-j)^2\} \tag{14}$$

where $g(i,j)$ denotes the element of GLCM.

The main steps for the proposed feature extraction method are given below.

a. Perform a 1-level two-dimensional DTCWT decomposition on input image, and use the high-pass coefficients to construct six sub-images, denoted as $I_{1,\alpha}$, where $\alpha = \{\pm\pi/12, \pm\pi/4, \pm5\pi/12\}$.

b. Obtain corresponding co-occurrence matrices for each $I_{1,\alpha}$, denoted as G_d^θ, where $d=\{1,2\}$ and $\theta=\{0,\pi/4,\pi/2,3\pi/4\}$.

c. Calculate *UNI*, *CON*, *ENT* and *INV* for each G_d^θ according to Eqs. (11)–(14).

d. Concatenate all of the statistical values obtained in step c, and implement normalization to construct the final feature vector.

4. Experiments and discussions

In this section, we perform extensive experiments on two commonly used natural texture image databases, i.e., MIT VisTex [30] and Brodatz [31], to evaluate the effectiveness of the proposed texture feature extraction method. 20 texture images (see Fig. 4) are selected respectively from the two texture databases. Since each texture image is one class, 20 classes can be obtained from each database. The original texture image has a size of 512×512 with 256 gray-levels, and is normalized to $[-1, 1]$. In our experiment, each texture image is subdivided into 64 non-overlapping image regions with a size of 64×64. Therefore, a total of 1280 sub-image regions are obtained in each database. To perform supervised classification, 640 sample sub-images are randomly used for training and the remaining 640 sample sub-images are applied for testing on each texture image database. All the experiments are performed on the platform of Lenovo M7100 (Dual core 2.83 GHz CPU and 4 GB RAM).

After feature extraction, LIBSVM package [32] is applied for our texture classification, and the confusion matrix (CM) is used to measure the classification performance. Assume that CM is a $M \times M$ matrix for M different texture classes, and $CM(i,j)$ refers to the classification rate when samples from class i are identified

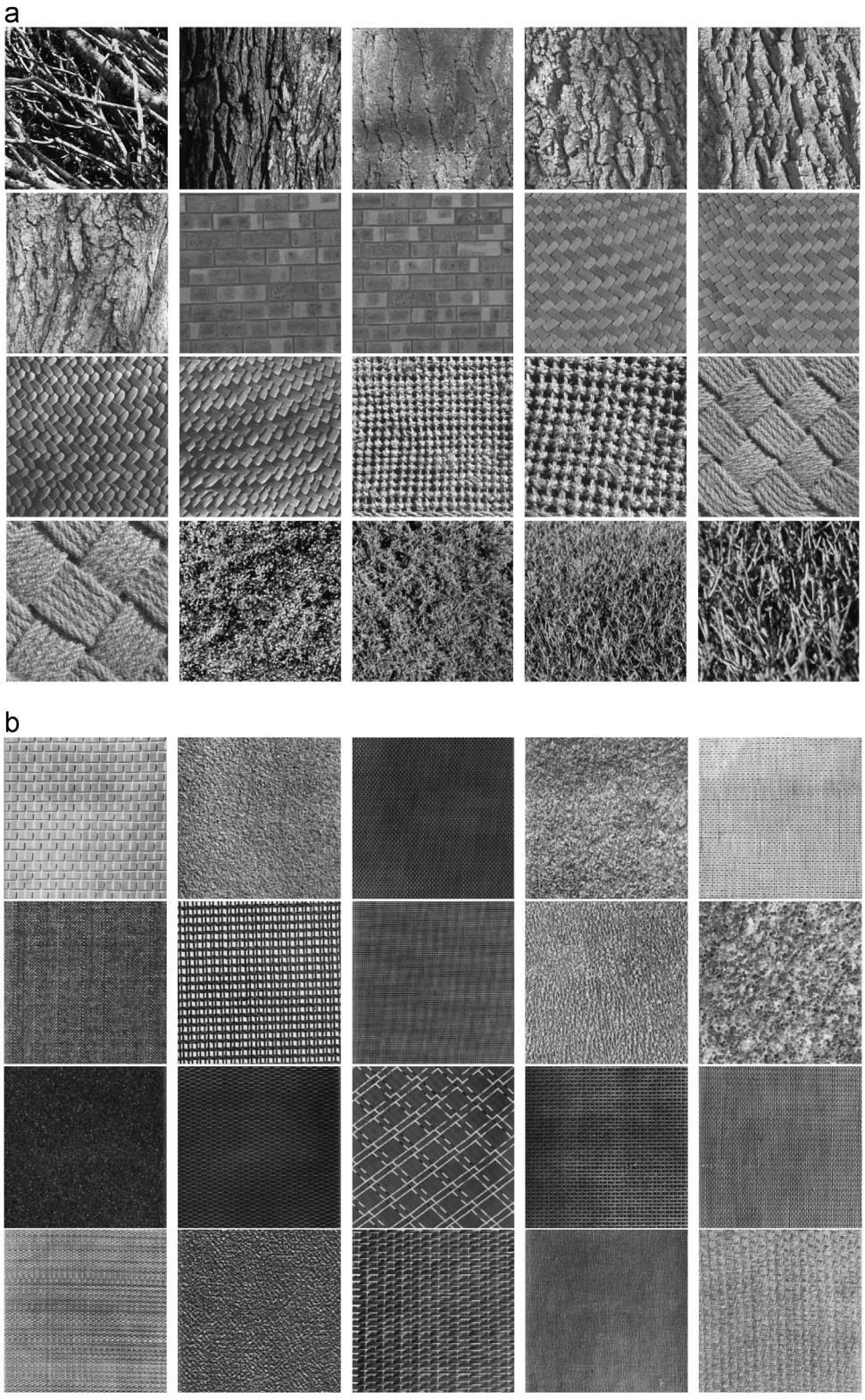

Fig. 4. Texture images from different databases (a) MIT VisTex (b) Brodatz.

as class j. The average correct classification rate ($accr$) and average false classification rate ($afcr$) are calculated as follows:

$$accr = \frac{1}{M} \sum_{\forall (i,j), i=j} CM(i,j) \tag{15}$$

$$afcr = \frac{1}{M(M-1)} \sum_{\forall (i,j), i \neq j} CM(i,j) \tag{16}$$

Table 1
Classification results of different filters for DTCWT. (using $d=2$, $\theta=0$, $\pi/4$, $\pi/2$, and $3\pi/4$ for GLCM).

Filters	*Accr* (%) on MIT VisTex	Afcr (%) on MIT VisTex	*Accr* (%) on Brodatz	Afcr (%) on Brodatz
Antonini 9,7 tap filters	97.85	0.45	95.5	2
LeGall 5,3 tap filters	98.65	0.34	97.15	1.87
Near-symmetric 5,7 tap filters	99.46	0.24	98.7	1.73
Near-symmetric 13,19 tap filters	99.93	0.14	98.82	1.6

Table 2
Classification results of different distances and angles for GLCM. (using near-symmetric 13,19 tap filters for DTCWT).

GLCM parameters	*Accr* (%) on MIT VisTex	Afcr (%) on MIT VisTex	*Accr* (%) on Brodatz	Afcr (%) on Brodatz
$d=1$, $\theta=0$, $\pi/4$, $d=2$, $\theta=0$, $\pi/4$	99.73	0.25	98.13	1.75
$d=1$, $\theta=0$, $\pi/2$, $d=2$, $\theta=0$, $\pi/2$	99.95	0.18	98.77	1.6
$d=1$, $\theta=0$, $\pi/4$, $\pi/2$, $3\pi/4$	99.18	0.5	98	1.73
$d=2$, $\theta=0$, $\pi/4$, $\pi/2$, $3\pi/4$	99.93	0.14	98.82	1.6

4.1. Selecting the filters for DTCWT

Since our proposed feature extraction method need perform DTCWT decomposition on a input texture image, the filters selection of DTCWT will affect the final classification effectiveness. Table 1 gives classification performance of the proposed feature extraction method using different filters for DTCWT decomposition. It is observed that $accr$ of 99.93% and $afcr$ of 0.14% are respectively achieved by using near-symmetric 13,19 tap filters on database MIT VisTex (98.82% and 1.6% on Brodatz), which yields the best classification results.

4.2. Selecting the directions and distances for GLCM

In the proposed method, GLCM has been used for feature extraction from the DTCWT domain of original image. Therefore, different combinations of distances and angles, which consider the most adjacent and close neighboring pixels for GLCM formation, have been observed in our experiment. The results of $accr$ and $afcr$ on the two test datasets have been shown in Table 2. It is observed that GLCM with $d=2$, and $\theta=\{0,\pi/4,\pi/2,3\pi/4\}$, gives better results for texture classification.

4.3. Analyzing the properties of the extracted feature vector

In this section, four texture images (Bark.0009 and Fabric.0002 in MIT VisTex, D01 and D34 in Brodatz) from the two test databases are selected to make insight about the structure of the extracted feature by using our proposed method. Note that GLCM can extract the spatial information between pixels, while DTCWT is approximately shift invariance and has good directional selectivity in two dimensions. Therefore, applying GLCM on DTCWT

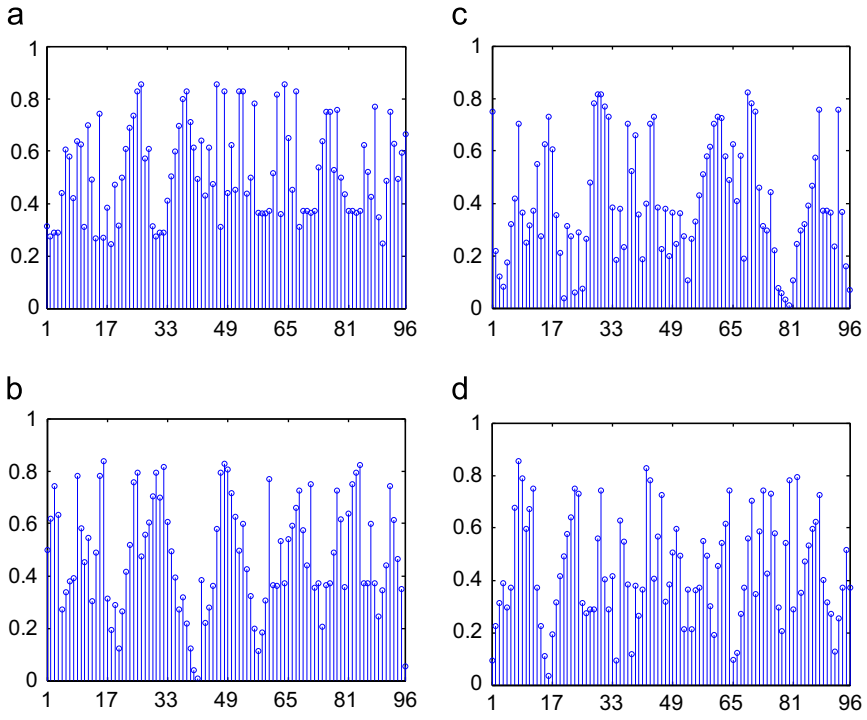

Fig. 5. Feature vector for 4 texture images (a) Bark.0009 (b) Fabric.0002 (c) D01 (d) D34.

Table 3
Classification results on MIT VisTex.

Texture image	Correct classification rate (%)							
	DCH	Gabor	DTCWT	Contourlet+GLCM	DWT+GLCM	DTCWT+GLCM	CS-LBP	CLSP
Bark.0003	90	90	91.18	100	94	100	94.19	95.03
Bark.0007	100	83.16	93.46	100	100	100	100	100
Bark.0008	90	89.1	88.21	100	100	100	100	100
Bark.0009	85	90.09	99	98.15	93	99.79	99.17	99.00
Bark.0010	95	90	88.63	100	100	100	100	100
Bark.0011	88	92.07	100	99.8	96.4	100	100	100
Brick.0000	93	82.17	89.2	100	100	100	100	100
Brick.0001	95.88	89.1	90.19	100	98.12	100	100	100
Fabric.0000	98	82.79	99.1	100	100	100	97.64	97.37
Fabric.0001	96	90	86.23	100	98.5	100	96.12	96.94
Fabric.0002	86.45	85	99	98.26	95.4	99.65	95.96	96.46
Fabric.0003	88.85	90	88.21	100	96	100	96.84	96.84
Fabric.0009	100	87.92	90.19	100	100	100	100	100
Fabric.0010	94.8	85.63	100	98.78	95.95	99.8	100	100
Fabric.0011	85	87.12	95.14	98.68	95	99.65	95.43	96.11
Fabric.0012	90	89.1	100	100	96	100	96.85	97.02
Leaves.0003	89	80.19	98.11	98.85	96	99.79	100	100
Leaves.0012	88.25	87.12	94.15	100	95	100	100	100
Leaves.0013	100	86.13	99.1	100	100	100	100	100
Leaves.0014	100	93.06	100	100	100	100	100	100

Table 4
Classification results on Brodatz.

Texture image	Correct classification rate (%)							
	DCH	Gabor	DTCWT	Contourlet+GLCM	DWT+GLCM	DTCWT+GLCM	CS-LBP	CLSP
D01	92	93.21	97.05	97.25	93.5	98.8	98.30	98.96
D04	100	88.36	97.45	100	100	100	100	100
D06	93	94.25	90.64	98.68	95	99.15	100	100
D09	89.25	85.69	86.63	97.2	90	99.68	97.40	97.84
D14	65	75.25	84.4	83.15	73	85.79	85.76	86.31
D17	90	87.45	88.2	100	100	100	100	100
D20	88	86.38	85.85	100	100	100	100	100
D21	94	92.45	99.16	98.25	95.5	99.8	100	100
D24	100	88.59	90	100	100	100	100	100
D28	75	78.36	84.16	93.58	83.5	100	95.76	95.92
D32	85	86	85	100	100	100	100	100
D34	85	83.05	89.32	93.85	93	95.79	96.00	96.00
D47	80	90.16	98.68	96.05	86	99.58	96.74	96.09
D52	100	88.64	90.32	100	100	100	100	100
D53	72.15	80.05	89	93.24	83.86	97.98	98.04	98.82
D55	90	93.88	95.32	100	94.59	100	100	100
D57	90	83.96	94	96.85	96	99.88	98.44	98.13
D65	90	85.43	100	100	96.89	100	100	100
D77	86	82.59	93.46	100	100	100	100	100
D82	85.88	90	87.86	96.48	89.12	99.89	100	100

domain makes it effectively to extract spatial information along with six orientations for texture image. Our method first decompose the input texture image by using DTCWT to generate six sub-images. Then four GLCMs of each sub-image are obtained, and four statistical features of each GLCM are calculated. Therefore, the length of final feature vector is $6 \times 4 \times 4 = 96$. As is shown in Fig. 5, the feature vector extracted by using our proposed method (using near-symmetric 13,19 tap filters for DTCWT, $d=2$, $\theta=0$, $\pi/4$, $\pi/2$, and $3\pi/4$ for GLCM) can provide powerful texture discrimination.

4.4. Comparison with other methods

The classification performance for each texture class of the two test databases is obtained by using different feature extraction methods such as DWT based co-occurrence histogram (DCH for short) and Gabor [20], DTCWT [26], Contourlet+GLCM and DWT+GLCM [10], CS-LBP [33] and CLSP [34]. For method of DCH, the Haar wavelet is used to decompose the texture image and obtain the corresponding co-occurrence histograms. A feature vector of size 384 is used for training and classification. For method of Gabor, the even-symmetric Gabor filter is used and the energy feature vector of size 16 is used for training and classification. For method of DTCWT, 3 levels of DTCWT with near-symmetric 13,19 tap filters at level 1 and Q-shift 10,10 tap filters at levels ≥ 2 is used to decompose the texture image. A feature vector of size 36 is used for training and classification. For methods of Contourlet+GLCM and DWT+GLCM, feature combining is first used to form a base feature vector, and after that stepwise regression is used as a feature selection method to determine the final feature vector for training and classification. For method of CS-LBP, the input image is first divided into cells with a 4×4 grid. For each cell, the operator with parameters $R=1$(radius), $N=8$ (number of neighboring pixels) and $T=0.01$ are introduced to extract feature, and a final feature vector of size 256 is used for

training and classification. For method of CLSP, the operator with parameters $R=1$(radius), $P=8$(number of neighboring pixels), $a=1$ and $b=0$ for calculating the threshold value, are introduced to extract feature, and a final feature vector of size 256 is used for training and classification. The experimental results are given in Tables 3 and 4, which clearly shows that our proposed method (denoted as DTCWT+GLCM) can obtain better results than the other methods. Note that the computation time of classification mainly depends on the feature size, Table 5 gives corresponding feature vector length and classification time by using different methods. Apparently, DTCWT+GLCM can achieve the moderate result.

The average results on the whole test database are shown in Fig. 6. The *accr* is 92.66%, 87.49%, 94.46%, 99.63%, 97.47%, 99.93%, 98.61% and 98.74% by using method of DCH, Gabor, DTCWT, Contourlet+GLCM, DWT+GLCM, DTCWT+GLCM, CS-LBP and CLSP on database MIT VisTex. Accordingly, the *afcr* is 7.14%, 12.5%, 5.4%, 0.23%, 1.52%, 0.14%, 0.16% and 0.16% respectively. The *accr* is 87.51%, 86.69%, 91.33%, 97.23%, 93.5%, 98.82%, 98.32% and 98.4% by using method of DCH, Gabor, DTCWT, Contourlet+GLCM, DWT+GLCM, DTCWT+GLCM, CS-LBP and CLSP on database Brodatz. Accordingly, the *afcr* is 12.45%, 14.7%, 8.66%, 3.11%, 6%, 1.6%, 2% and 1.7% respectively.

Table 5
Classification times of different methods.

Method	Feature vector length	Average classification time (s)
DCH	384	1.8232
Gabor	16	0.1023
DTCWT	36	0.1230
Contourlet+GLCM	78	0.2925
DWT+GLCM	59	0.2490
DTCWT+GLCM	96	0.3250
CS-LBP	256	0.9335
CLSP	256	0.9525

It is observed that methods DCH, Gabor and DTCWT are overall inferior to the other five methods for texture classification. The reason is that they extract features directly through unique transform, which preserves the instinct shortcoming. Since DTCWT is a special case of the Gabor filters with complex coefficients, it has the directional advantages while requiring less computation. Furthermore, it is better than DWT as it is approximately shift invariance as well as directional selectivity. Therefore, DTCWT outperforms DCH and Gabor for feature extraction. Now we focus on the remaining five methods. In comparison with the other methods (i.e., DTCWT+GLCM, CS-LBP and CLSP), Contourlet+GLCM and DWT+GLCM can achieve comparable performance. However, they are sensitive to test database due to the simple feature fusion scheme. For example, the *accr* by using DWT+GLCM on MIT VisTex is 97.47%. While applying DWT+GLCM on Brodatz, the *accr* dramatically decreases to 93.5%. Compared to CS-LBP and CLSP, DTCWT+GLCM gives either better or comparable performance for most of the test cases, and one can find that DTCWT+GLCM is especially suited to handle images with strong directional texture (such as Bark.0003, Fabric.0000, Fabric.0001, Fabric.0002, Fabric.0003, Fabric.0011, Fabric.0012, D09, D28, D47 and D57). The reason is that DTCWT+GLCM uses GLCM to extract features on sub-images resulting from DTCWT decomposition, which can utilize both local mutual occurrence of patterns and global directional texture information for classification.

4.5. Robust evaluation

In this section, the cross validation is used to determine the robust of the extracted features by different methods described in Section 4.4. As mentioned above, 32 sub-images are randomly selected for training from each class while the remaining ones are used as testing set. On each database, the process iterates 100 times for different training samples, and the corresponding classification results are obtained for each method. Fig. 7 gives the interesting results on images Bark.0009, Fabric.0002, D01 and D34. It is observed that the proposed DTCWT+GLCM can obtain stable

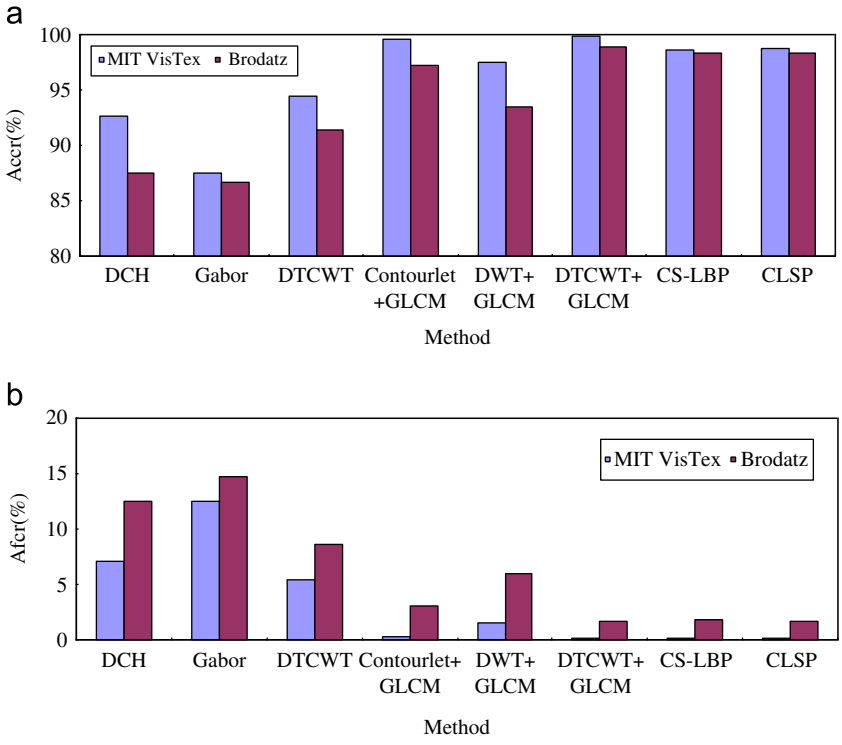

Fig. 6. Classification results by using different feature extraction methods on the two test databases. (a) *accr* (b) *afcr*.

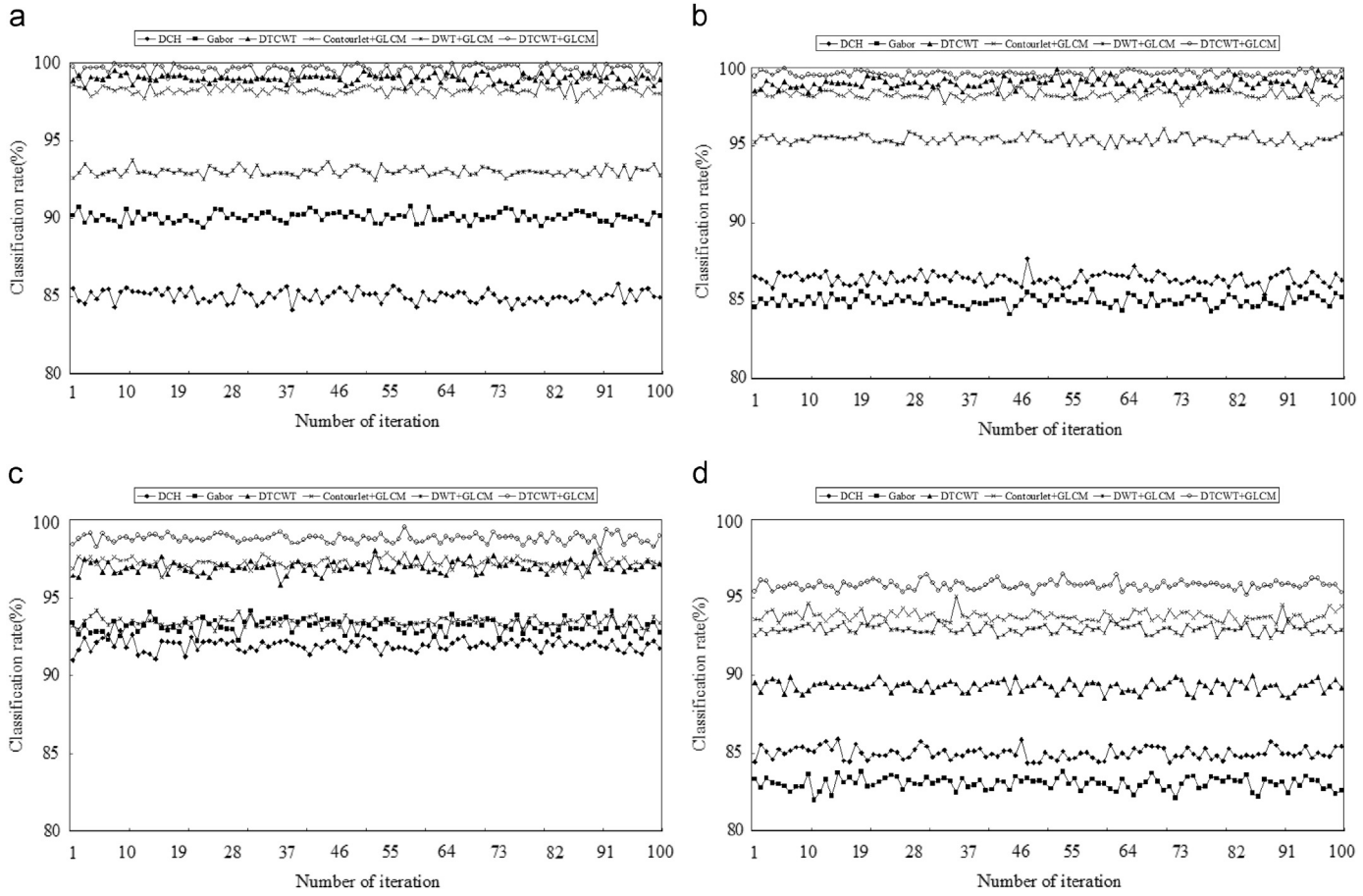

Fig. 7. Robust evaluation for 4 texture images (a) Bark.0009 (b) Fabric.0002 (c) D01 (d) D34.

correct classification rate than the other transform based methods over all training sets.

5. Conclusion

Recently, DTCWT has been proposed as a novel analysis tool for texture feature extraction since it has the advantages of low computation with limited redundancy, approximately shift invariance and directional selectivity compared to the conventional techniques such as DWT, Gabor and Contourlet. In this paper, a DTCWT based feature extraction method in conjunction with GLCM (denoted as DTCWT+GLCM) is proposed. Such method extracts the GLCM statistical features for texture classification from sub-images resulting from DTCWT decomposition, which is different from the traditional methods by directly using entropy, mean, variance or energy of the sub-images as the features. The experimental results show that the proposed method achieves average correct classification rate of 99.93% and 98.82% on test database VisTex and Brodatz respectively, which is better than several existing methods. To further enhance texture classification performance, some variants of SVM, such as GEPSVM [35], will be included in our future research.

Acknowledgments

We are grateful to the referees for their valuable comments. This work is financially supported by the National Natural Science Foundation of China (61363050, 61272077, 61563037), and the Natural Science Foundation of JiangXi Province (20142BDH80026).

References

[1] S.C. Kim, T.J. Kang, Texture classification and segmentation using wavelet packet frame and Gaussian mixture model, Pattern Recognit. 40 (4) (2007) 1207–1221.
[2] R.M. Haralick, K. Shanmugam, I. Dinstein, Textural features for image classification, IEEE Trans. Syst. Man Cybern. 3 (6) (1973) 610–621.
[3] M. Partio, B. Cramariuc, M. Gabbouj, A. Visa, Rock texture retrieval using gray level co-occurrence matrix 2002, in: Proceedings of the 5th Nordic Signal Processing Symposium, 2002.
[4] Qinggang Wu, Jubai An, Bin Lin, A texture segmentation algorithm based on pca and global minimization active contour model for aerial insulator images, IEEE J. Sel. Top. Appl. Earth Obs. Remote Sens. 5 (5) (2012) 1509–1518.
[5] Y. Zhang, S. Wang, G. Ji, P. Phillips, Fruit classification using computer vision and feedforward neural network, J. Food Eng. 143 (6) (2014) 167–177.
[6] F.R. Siqueira, W.R. Schwartz, H. Pedrini, Multi-scale gray level co-occurrence matrices for texture description, Neurocomputing 120 (10) (2013) 336–345.
[7] M. Subrahmanyam, Q.M.J. Wu, R.P. Maheshwari, R. Balasubramanian, Modified color motif co-occurrence matrix for image indexing and retrieval, Comput. Electr. Eng. 39 (3) (2013) 762–774.
[8] N. Jhanwar, S. Chaudhuri, G. Seetharaman, B. Zavidovique, Content based image retrieval using motif cooccurrence matrix, Image Vis. Comput. 22 (14) (2004) 1211–1220.
[9] J. Zhang, G. Li, S. He, Texture-based image retrieval by edge detection matching GLCM, in: Proceedings of the 10th IEEE International Conference on High Performance Computing and Communications, 2008, pp. 782–786.
[10] S.K. Vipparthi, S.K. Nagar, Multi-joint histogram based modeling for image indexing and retrieval, Comput. Electr. Eng. 40 (8) (2014) 163–173.
[11] Ibrahim Jarrar, Khaled Assaleh, Ayman H. El-Hag, Using a pattern recognition-based technique to assess the hydrophobicity class of silicone rubber materials, IEEE Trans. Dielectr. Electr. Insul. 21 (6) (2014) 2611–2618.
[12] R. Panda, B.N. Chatterji, Unsupervised texture segmentation using tuned filters in Gaborian space, Pattern Recognit. Lett. 18 (5) (1997) 445–453.

[13] S. Arivazhagan, L. Ganesan, S. Padam Priyal, Texture classification using Gabor wavelets based rotation invariant features, Pattern Recognit. Lett. 27 (16) (2006) 1976–1982.
[14] Q. Yin, J.N. Kim, K.S. Moon, Rotation invariant texture classification using gabor wavelets, Lect. Notes Comput. Sci. 4489 (2007) 10–17.
[15] Aun Irtaza, M. Arfan Jaffar, Categorical image retrieval through genetically optimized support vector machines (GOSVM) and hybrid texture features, Signal Image Video Process. 9 (2014) 1503–1519.
[16] S. Arivazhagan, L. Ganesan, Texture classification using wavelet transform, Pattern Recognit. Lett. 24 (2) (2003) 1513–1521.
[17] K. Muneeswaran, L. Ganesan, S. Arumugam, K.R. Soundara, Texture classification with combined rotation and scale invariant wavelet features, Pattern Recognit. 38 (10) (2005) 1495–1506.
[18] Minh N. Do, Martin Vetterli, Wavelet-based texture retrieval using generalized gaussian density and Kullback–Leibler distance, IEEE Trans. Image Process. 11 (2) (2002) 146–158.
[19] S.C. Kim, T.J. Kang, Texture classification and segmentation using wavelet packet frame and Gaussian mixture model, Pattern Recognit. 40 (4) (2002) 1207–1221.
[20] M. Kokare, P.K. Biswas, B.N. Chatterji, Texture image retrieval using rotated wavelet filters, Pattern Recognit. Lett. 28 (10) (2007) 1240–1249.
[21] P.S. Hiremath, S. Shivashankar, Wavelet based co-occurrence histogram features for texture classification with an application to script identification in a document image, Pattern Recognit. Lett. 29 (9) (2008) 1182–1189.
[22] Y. Zhang, S. Wang, P. Sun, P. Phillips, Pathological brain detection based on wavelet entropy and Hu moment invariants, Bio-Med. Mater. Eng. 26 (S) (2015) 1283–1290.
[23] M.N. Do, V. Martin, The contourlet transform: an efficient directional multiresolution image representation, IEEE Trans. Image Process. 14 (12) (2005) 2091–2106.
[24] N.G. Chitaliya, A.I. Trivedi, An efficient method for face feature extraction and recognition based on contourlet transforms and principal component analysis, Procedia Comput. Sci. 2 (6) (2010) 52–61.
[25] P. Ganasala, V. Kumar, CT and MR image fusion scheme in nonsubsampled contourlet transform domain, J. Digit. Imaging 27 (3) (2014) 1–12.
[26] N.G. Kingsbury, Complex wavelets for shift invariant analysis and filtering of signals, J. Appl. Comput. Harmonic Anal. 10 (3) (2001) 234–253.
[27] J. Fauqueur, N. Kingsbury, R. Anderson, Semantic discriminant mapping for classification and browsing of remote sensing textures and objects, in: proceedings of the IEEE International Conference on Image Processing, 2005, pp. 846–849.
[28] T. Celik, T. Tjahjadi, Multiscale texture classification using dual-tree complex wavelet transform, Pattern Recognit. Lett. 30 (3) (2009) 331–339.
[29] P. Kennel, C. Fiorio, F. Borne, Supervised image segmentation using Q-Shift dual-tree complex wavelet transform coefficients with a texton approach, Form. Pattern Anal. Appl. 18 (2015) 1–11.
[30] MIT Vision and Modeling Group. [Online]. Available: ⟨http://vismod.media.mit.edu/pub/VisTex⟩.
[31] ISRN Machine Vision. [Online]. Available: ⟨http://multibandtexture.recherche.usherbrooke.ca/original_brodatz.html⟩.
[32] LIBSVM – A Library for Support Vector Machines. [Online]. Available: ⟨http://www.csie.ntu.edu.tw/~cjlin/libsvm/index.html⟩.
[33] M. Heikkilä, M. Pietikäinen, C. Schmid, Description of interest regions with local binary patterns, Pattern Recognit. 42 (3) (2009) 425–436.
[34] Nishant Shrivastava, Vipin Tyagi, An effective scheme for image texture classification based on binary local structure pattern, Vis. Comput. 30 (11) (2014) 1223–1232.
[35] Y. Zhang, Z. Dong, S. Wang, G. Ji, J. Yang, Preclinical diagnosis of magnetic resonance (MR) brain images via discrete wavelet packet transform with tsallis entropy and generalized eigenvalue proximal support vector machine (GEPSVM), Entropy 17 (4) (2015) 1795–1813.

Peng Yang received the M.Sc. degree in computer applications technology from the Wuhan University of Technology, Hubei, China, in 2006, and the Ph. D. degree in computer science and technology from the Chongqing University, Chongqing, China, in 2010. Currently, he is an associate professor in School of Information Engineering, Nanchang Hangkong University, Jiangxi, China. His current research interests include image processing, pattern recognition and data mining, etc.

Guowei Yang received the B.Sc. degree and the M.Sc. degree in mathematics from the Jiangxi Normal University, Nanchang, China, in 1985 and 1988, and the Ph. D. degree from the University of Science and Technology Beijing, China, in 2004. He was appointed as Professor in the Qingdao University, China, in1999. His current research interests include artificial intelligence, artificial life, artificial neural network, pattern recognition, innovative and creative design, etc.